Coulometric ion sensing with Li^+-selective $LiMn_2O_4$ electrodes

Lyu, Yan; Han, Tingting; Zhong, Lijie; Tang, Yitian; Xu, Longbin; Ma, Yingming; Bao, Yu; Gan, Shiyu; Bobacka, Johan; Niu, Li

Published in:
Electrochemistry Communications

DOI:
10.1016/j.elecom.2022.107302
10.1016/j.elecom.2022.107302

Published: 01/01/2022

Document Version
Final published version

Document License
CC BY-NC-ND

Electrochemistry Communications 139 (2022) 107302

Contents lists available at ScienceDirect

Electrochemistry Communications

journal homepage: www.elsevier.com/locate/elecom

Full Communication

Coulometric ion sensing with Li^+-selective $LiMn_2O_4$ electrodes

Yan Lyu [a,b], Tingting Han [a], Lijie Zhong [a], Yitian Tang [a], Longbin Xu [a], Yingming Ma [a], Yu Bao [a], Shiyu Gan [a,*], Johan Bobacka [b,*], Li Niu [a]

[a] School of Civil Engineering, c/o Guangzhou Key Laboratory of Sensing Materials & Devices, Center for Advanced Analytical Science, School of Chemistry and Chemical Engineering, Guangzhou University, Guangzhou 510006, China

[b] Laboratory of Molecular Science and Engineering, Johan Gadolin Process Chemistry Centre, Åbo Akademi University, Henriksgatan 2, FI-20500 Åbo, Finland

ARTICLE INFO

Keywords:
Coulometric signal readout
Solid-contact ISEs
Membrane-free ISEs
$LiMn_2O_4$

ABSTRACT

A coulometric signal readout method, which was originally developed for solid-contact ion-selective electrodes, was investigated in this work using $LiMn_2O_4$ (LMO) as a combined ion-recognition and signal-transduction layer. The redox process of LMO, which is associated with reversible intercalation/expulsion of Li^+ ions, allowed coulometric sensing of Li^+ ions in aqueous solutions. On increasing the active area (mass loading) of LMO, the coulometric signal increased for a given change in Li^+ ion activity. The excellent redox reversibility of LMO and its relatively low resistance were instrumental in achieving a high signal amplification together with a relatively fast response. Coating the LMO layer with a conventional Li^+-selective plasticized PVC membrane was found to dramatically lower the coulometric response. Hence, the application of LMO as a combined Li^+-selective electrode material and ion-to-electron transducer was found to be highly compatible with the coulometric signal readout method, especially for detecting small Li^+ activity changes at high Li^+ concentrations.

1. Introduction

Solid-contact ion-selective electrodes (SC-ISEs) are important chemical sensors used in a wide range of modern applications, such as wearable sensors for monitoring pH and electrolytes [1–3], as well as for on-site environmental monitoring [4,5]. The demands for portability and excellent sensitivity of ion sensors are constantly increasing, motivating the investigation of new sensor materials and new detection principles beyond potentiometry [6–12]. In 2015, a coulometric signal transduction method was introduced to overcome the limiting sensitivity of traditional potentiometric sensing that is essentially defined by the Nernstian slope, i.e., 59.2 mV/dec for a monovalent cation. By transferring the voltage signal to a current that can be integrated to obtain the charge it is possible to amplify the signal for a given change in analyte concentration [8,9,13]. The coulometric readout for SC-ISEs has been mostly studied using a conducting polymer coated with a plasticized PVC-based ion-selective membrane [8,9,13–15]. This type of SC-ISE generally shows a relatively slow coulometric response due to the high resistance of the ion-selective membrane (ISM), even for thin-layer ISMs.

Recently, SC-ISEs without a plasticized PVC-based membrane have attracted some attention, as discussed in our previous work [16–19]. Unlike PVC membrane-based SC-ISEs, the membrane-free SC-ISEs have only two phase boundaries (substrate|SC, SC|aq), where the first phase boundary provides electron transfer and the second plays a role in ion transfer. This single-piece structured system shows potential for building stable, portable, and low-cost sensor systems [17,19,20]. Here, the solid contact layer plays a role in both specific ion recognition and ion-to-electron transduction, which requires a material showing both ion selectivity and reversible redox electrochemistry. Lithium manganese oxide ($LiMn_2O_4$, spinel structure) is a type of classical lithium battery material in which Mn cations occupy the octahedral interstices and Li is located in tetrahedral interstices (Fig. 1) [21–23]. The unique three-dimensional network provides fast transport of Li^+ ions while maintaining the original structure by changing valence of Mn (Mn (3.5) ↔ Mn (4.0)) [24–26]. Hedman and Björefors recently studied fiber optic evanescent wave (FOEW) sensors for monitoring the dynamic environment of $LiMn_2O_4$ cathodes in pouch cells [27]. Suherman et al. used a $LiMn_2O_4$-modified screen-printed electrode to detect Li^+ in authentic human saliva through linear stripping voltammetry (LSV) [24]. Additionally, recent studies by our group show that $LiMn_2O_4$ gives a Nernstian potentiometric response to Li^+ ions with excellent selectivity against Na^+ ($\log K_{Li,Na} = -4.1$), K^+ ($\log K_{Li,K} = -3.7$), Ca^{2+} ($\log K_{Li,Ca} = -4.3$), and Mg^{2+} ($\log K_{Li,Mg} = -4.2$) [16].

* Corresponding authors.
E-mail addresses: ccsygan@gzhu.edu.cn (S. Gan), johan.bobacka@abo.fi (J. Bobacka).

https://doi.org/10.1016/j.elecom.2022.107302
Received 13 March 2022; Received in revised form 24 May 2022; Accepted 25 May 2022
Available online 27 May 2022

In this work, we investigated the coulometric signal readout method for membrane-free SC-ISEs, taking $LiMn_2O_4$ deposited on glassy carbon (GC/LMO) as an example, as illustrated schematically in Fig. 1. In the coulometric method, the potential of the SC-ISE is held constant vs. the reference electrode (RE). When there is a change in the solution concentration (activity) of the primary ion, a potential difference will arise between the SC-ISE and RE [8,13]. As a result of this potential difference, a transient current will flow between the SC-ISE and the counter electrode, causing oxidation/reduction of the SC material, and then the current returns to zero as soon as a new equilibrium is reached [13,14,28]. In the case of the GC/LMO electrodes used in this work, the transient current originates from the following redox reaction: $LiMn_2O_4 \leftrightarrow Li_{1-x}Mn_2O_4 + xLi^+ + xe^-$, as illustrated in Fig. 1. The experimental results provide evidence of the successful application of coulometric signal transduction for membrane-free SC-ISEs based on GC/LMO.

2. Experimental

2.1. Materials

$LiMn_2O_4$ (LMO, 99.5%, metal basis, spinel structure) was purchased from Alfa Aesar, China. Poly(vinylidene fluoride) (PVDF, molecular weight ~ 53400) and N-methyl pyrrolidone (NMP, anhydrous, ≥ 99.9%) were obtained from Sigma-Aldrich, USA. Lithium chloride (LiCl, ≥ 99.0%, anhydrous) was supplied by Sigma-Aldrich (USA) and used in preparing the primary ion solution. Lithium ion ionophore VI, high molecular weight PVC (poly(vinyl chloride)), potassium tetrakis(*p*-chlorophenyl)borate (KTpClPB), bis(2-ethylhexyl) sebacate (DOS), and tetrahydrofuran (THF) were all purchased from Sigma-Aldrich, USA. Glassy carbon disk electrodes and aluminium oxide (Al_2O_3) polishing powder were supplied by Tianjin Aida Heng sheng Technology Co. Ltd, China. Nitrogen gas (N_2, 99.9995%) was purchased from Guangdong Liquefied Air Co. Ltd, China. All standards and aqueous solutions were prepared with analytical grade chemicals in deionized water (resistivity ≥ 18.2 MΩ cm), which was produced using an ultra-pure water system from Sichuan Waterpure Instrument Co. Ltd, China.

2.2. Preparation of ion-selective electrodes

Glassy carbon (GC) disk electrodes with an electrode diameter of 5 mm (in a Teflon shell) were used as the substrate for the working electrodes in this study. The GC disk electrodes were polished using a polishing cloth with 0.3 and 0.05 μm Al_2O_3, after which they were cleaned sequentially with deionized water and ethanol, and finally dried under a flow of nitrogen gas.

2.2.1. Fabrication of membrane-free GC/LMO electrodes

GC/LMO electrodes were prepared by drop-casting 4, 7, or 12 μL of LMO suspension onto the GC disk electrode surface, followed by drying at 60 ℃ for 4 h. Typically, the LMO suspension consisted of a mixture of LMO material and PVDF binder (weight ratio = 8:2), obtained after ultrasonicating in NMP for 2 h. The concentration of LMO in NMP was 50 mg/mL. All GC/LMO electrodes were conditioned in 0.1 M LiCl solution overnight before use.

2.2.2. Fabrication of GC/LMO/ISM electrodes

The Li^+ membrane cocktail contained 32.9 wt% PVC, 0.4 wt% KTpClPB, 65.7 wt% DOS and 1 wt% lithium ionophore VI, with a total mass of 100 mg dissolved in 1 ml THF. The GC/LMO/ISM electrodes were fabricated by drop-casting 50 μL of membrane cocktail solution onto the surface of the GC/LMO electrodes and then drying overnight at room temperature.

2.3. Electrochemical measurements

The prepared GC/LMO electrodes, a saturated calomel electrode (SCE) and a bare glassy carbon rod were used as the working electrode, reference electrode and counter electrode, respectively. The performance of the GC/LMO electrodes was checked by potentiometric measurements before conducting chronoamperometric and coulometric experiments. Cyclic voltammetry was performed with an Iviumstat instrument (Ivium Technologies, The Netherlands) in a three-electrode system in 1 M LiCl solution. The scan rate was 1 mV s^{-1} in a potential range from 0 to 1.4 V. Potentiometric measurements of the GC/LMO electrodes were recorded by a 16-channel mV-meter (Lawson Laboratories Inc., input impedance = 10^{15} Ω) at room temperature. All electrodes were conditioned in 10^{-3} M LiCl solution overnight and then transferred into 10^{-7} M LiCl solution for 4 h before the potentiometric measurements.

Chronoamperometric measurements were performed using the Iviumstat, while shielding the electrochemical cell in a Faraday cage to decrease unwanted noise. In this study, the potential of the GC/LMO

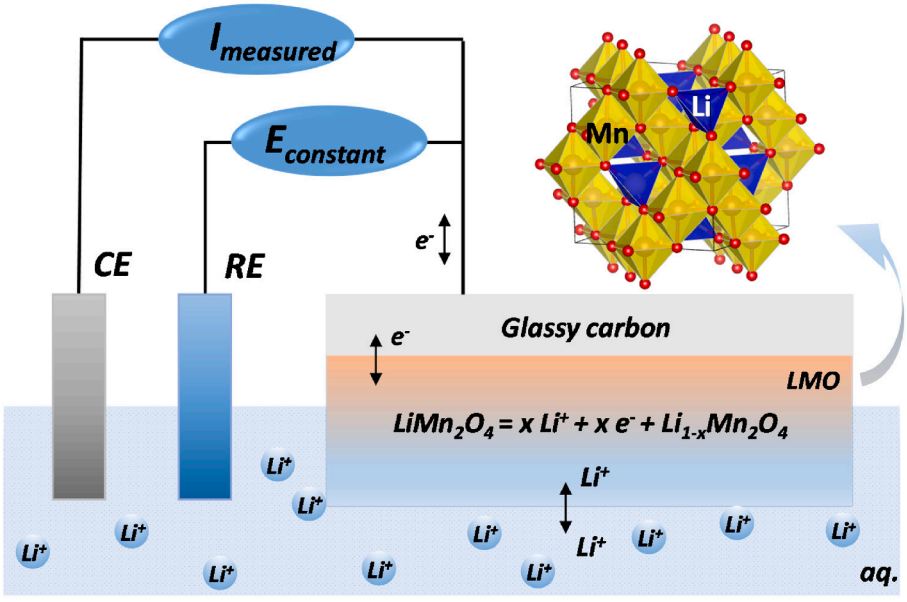

Fig. 1. Schematic illustration of the coulometric signal readout method for the membrane-free GC/LMO electrode. The potential of the GC/LMO is kept constant vs. the reference electrode (RE). Whenever there is a change in the Li^+ ion activity in the solution, a transient current signal (current peak) is recorded between the GC/LMO and the counter electrode (CE) due to oxidation/reduction of $LiMn_2O_4$ (LMO) with simultaneous Li^+ transport from/into the LMO crystal lattice. Integration of the transient current gives the charge, which is the analytical signal.

electrode was set to a constant value that was equal to the open circuit potential vs. RE in the starting solution, while measuring the current between the GC/LMO and the counter electrode. The measurements were done using automatic dilution with a 700 Dosino/711 Liquino system (Metrohm): the starting concentration of the primary ion was 0.1 M LiCl, followed by a dilution step of 0.13, 0.06, and 0.03 dec/step with deionized water or 0.1 M NaCl (when using 0.1 M NaCl as an ionic background solution). The coulometric signal was obtained by integrating the chronoamperometric curve. The dilution procedure took approximately 10 ~ 30 s for each dilution step. Electrochemical impedance spectroscopy (EIS) was performed using a Gamry reference 600 plus workstation in 1 M LiCl and a three-electrode system at open circuit potential (OCP). The frequency range used was from 1 MHz to 0.1 Hz with an ac-amplitude of 10 mV.

3. Results and discussion

3.1. Potentiometric, amperometric and coulometric response of the GC/LMO

GC/LMO electrodes were fabricated by drop-casting 7 μL of LMO suspension onto the surface of GC electrodes. First, the GC/LMO electrodes were investigated in the potentiometric mode in LiCl solutions from a concentration of 10^{-7} M to 10^{-1} M with a step of $\Delta\log a_{Li+} = 1$ dec/step. As shown in Fig. S1, the GC/LMO gave a linear potentiometric response with a slope of 56 ± 1.4 mV/dec from 10^{-1} to $10^{-4.5}$ M LiCl. The concentration was altered by successive manual additions of LiCl solution. To assess if the GC/LMO electrodes could be used in coulometric measurements, chronoamperometric and coulometric curves were recorded in LiCl solution from 10^{-6} M to 10^{-1} M at $\Delta\log a_{Li+} = 1$ dec/step (Figs. S2a and S2b). A constant potential (equal to OCP vs. RE in 10^{-6} M LiCl) was applied to the GC/LMO electrode in10^{-6} M LiCl solution until equilibrium was established, i.e., the recorded current was within ± 10 nA for 10 min. Only a minor current response was observed when the LiCl solution was changed from 10^{-6} to 10^{-5} M (Fig. S2a). An increase in Li^+ concentration (increase in potential at the LMO/solution interface) will cause a reduction of the LMO material together with an influx of Li^+ ions from the solution to the LMO to maintain electroneutrality ($Li_{1-x}Mn_2O_4 + xLi^+ + xe^- \rightarrow LiMn_2O_4$). The small amperometric response observed when increasing the Li^+ concentration from 10^{-6} to 10^{-5} M can thus be related to ion transport limitations in solution and to the weak concentration gradient at low concentrations, which is insufficient to drive diffusion [16]. A current response was observed when going from 10^{-5} to 10^{-4} M (Fig. S2a) but the electrode did not reach equilibrium within 5 min, i.e., the coulometric curve did not reach a plateau (Fig. S2b). This can again be ascribed to the low diffusion rate of lithium ions in LMO at low concentrations in solution. As reported earlier, the LMO layer is responsible for both recognition and transduction of the target Li^+ ion from and to the analytical solution through the crystal lattice of LMO, which is a time-dependent process [16]. Therefore, it must also be kept in mind that the GC/LMO electrode has a detection limit of $10^{-4.5}$ M and a sub-Nernstian response between 10^{-5} and 10^{-4} M in potentiometric measurements (Fig. S1), which will naturally limit the amperometric and coulometric response at low concentrations (below 10^{-4} M LiCl). A large current peak was observed when the LiCl concentration was increased from 10^{-4} to 10^{-3} M. The current peak became larger and sharper as the concentration was increased further to 10^{-2} and 10^{-1} M, indicating a stronger driving force to Li^+ at higher LiCl concentrations (Fig. S2a). The concentration change from 10^{-2} to 10^{-1} M presented the sharpest transient current, demonstrating the fast coulometric response of GC/LMO electrodes at high concentrations of LiCl (Fig. S2b). These experimental results suggested that the coulometric method works for GC/LMO at high Li^+ concentrations.

Fig. 2 shows the chronoamperometric and coulometric response of GC/LMO (mass loading of LMO = 12 μL) upon 15 successive dilutions, in which the dilution step was 0.03 dec per step from a starting concentration of 0.1 M LiCl. During each dilution step, a positive current was observed as LMO was further oxidized ($LiMn_2O_4 \rightarrow Li_{1-x}Mn_2O_4 + xLi^+ + xe^-$), with simultaneous Li^+ deintercalation through the crystal pathways and release of Li^+ into the aqueous solution. Reproducible current peaks and integrated charge (Q) values were observed, as shown in Fig. 2(a) and 2(b). A slope of −286.1 ± 15.6 μC/dec was obtained. Both the current peaks and the observed linearity of Q with $\log a_{Li+}$ confirmed the successful application of the coulometric signal readout method for GC/LMO at small concentration changes. The above electrodes were conditioned in 0.1 M LiCl before use. Such electrode conditioning is a traditional procedure for ISEs. ISEs conditioned in a solution that contains the primary ion show stable and reproducible electrode behavior, and this is recommended for practical use of the sensor. To test the performance of an unconditioned electrode, GC/LMO electrodes without conditioning were tested in the starting solution of 0.1 M LiCl, $\Delta\log a_{Li+} = 0.03$ dec/step, as shown in Fig. S3. From Fig. S3(a) we can observe increasing current peaks in successive measurements. This shows that the response of the electrode gradually changes after first contact with the solution and the current did not return to the baseline in 5 min after each dilution step. As a consequence, the cumulative Q value did not stabilize after each dilution step and the calibration curve was nonlinear (Fig. S3b). Therefore, we preferred to condition the electrodes before making any measurements.

Based on the response mechanism involving Li^+ intercalation/deintercalation in the LMO lattice, a decrease in the LMO crystal active area in contact with the electrolyte should allow faster ion recognition and re-equilibration, if the redox process of LMO is limited by mass transport inside the crystalline structure of LMO. To evaluate the influence of mass transport in LMO, coulometric readout measurements for GC/LMO electrodes with different LMO active areas (mass loading) were performed.

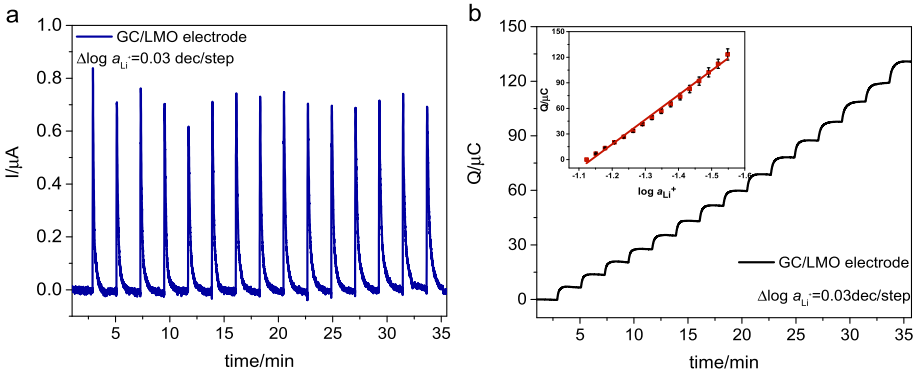

Fig. 2. (a) Chronoamperograms for GC/LMO and (b) corresponding integrated charge Q with $\Delta\log a_{Li+} = 0.03$ dec/step, in which the inset image is the fitting line of Q vs. ion activity ($n = 3$). The starting concentration of the primary ion was 0.1 M LiCl.

3.2. Amperometric and coulometric response of GC/LMO with different LMO active areas

The influence of the LMO active area in contact with the electrolyte on the response of the GC/LMO electrodes was studied. Three types of GC/LMO electrodes with different active areas were prepared by drop-casting 12 μL, 7 μL and 4 μL of LMO suspension onto the surface of GC electrodes, and then drying them in an oven for 4 h at 60 ℃. All GC/LMO electrodes were conditioned in 0.1 M LiCl overnight before use to reach equilibrium ion conditions. Fig. 3 shows the response of the three types of GC/LMO electrodes with three different dilution steps (Δlog a_{Li+}= 0.13, 0.06, and 0.03 dec/step, respectively), starting with a solution of 0.1 M LiCl. For a given dilution step, the current response and integrated Q increased with increasing active area of the LMO, which is the reason for the signal amplification in the coulometric readout mode. As the LMO active area increased, the response time of the amperometric and coulometric response also increased. Hence, the GC/LMO electrodes with the highest active area provided the highest current peaks and cumulative charge, but the slowest response. This result is ascribed to the sensing mechanism of the coulometric readout for the LMO material, which plays a role in both recognition and transduction through crystal pathways. Each successive dilution of the LiCl solution caused a potential decrease at the LMO/solution interface (Nernst equilibrium). Since the potential of the GC/LMO vs. the reference electrode was held constant, the potential drop at the LMO/solution interface was compensated by oxidation of Mn (3.5) to Mn (4.0) in the LMO material [25,29,30]. In order to maintain electroneutrality, Li^+ ions were expelled into the aqueous solution. On increasing the active area of the LMO, there was a longer diffusion distance for Li^+ ions to travel inside the LMO layer (between grains), which meant a longer time (bigger integrated Q) to reach the new equilibrium. Thus, increasing the active area of the LMO is one way to amplify the coulometric charge (Q) readout. It should be stressed that all the GC/LMO electrodes tested (except for 12 μL, Δlog a_{Li+} = 0.13 dec/step) were able to equilibrate in 4 min for the Δlog a_{Li+} = 0.13 dec/step, in 3 min for the Δlog a_{Li+} = 0.06, dec/step, and in 2 min for the Δlog a_{Li+} = 0.03 dec/step. The transient current in the chronoamperometric measurement correlated with the electrode impedance, i.e., the LMO produced with a mass loading of 12 μL possessed the highest impedance (Fig. S4).

Figure S5 shows three cyclic voltammograms for GC/LMO electrodes with a mass loading (active area) of 12 μL, 7 μL and 4 μL in the potential range from 0 to 1.4 V vs. SCE at a scan rate of 1 mV s^{-1} in 1 M LiCl solution. Two pairs of peaks can be observed at 0.79/0.75 V and 0.91/0.88 V, which correspond to intercalation and de-intercalation processes of Li^+ at the LMO/solution phase boundary [31–33]. In addition, no obvious potential shifts of the oxidation and reduction peaks were observed at these different mass loadings, indicating the excellent Li^+ transfer performance of the LMO material. GC/LMO shows capacitive behavior within the potential range ca 0.3–0.6 V (Fig. S5), which covers the potential span of the potentiometric response of GC/LMO (Fig. S1). For a certain mass loading (active area), the response time of the GC/LMO decreases on decreasing the dilution step, accompanied by a lower transient current peak and cumulative charge (Fig. 4). For example, the response of the GC/LMO (7 μL LMO loading) to a small dilution step of

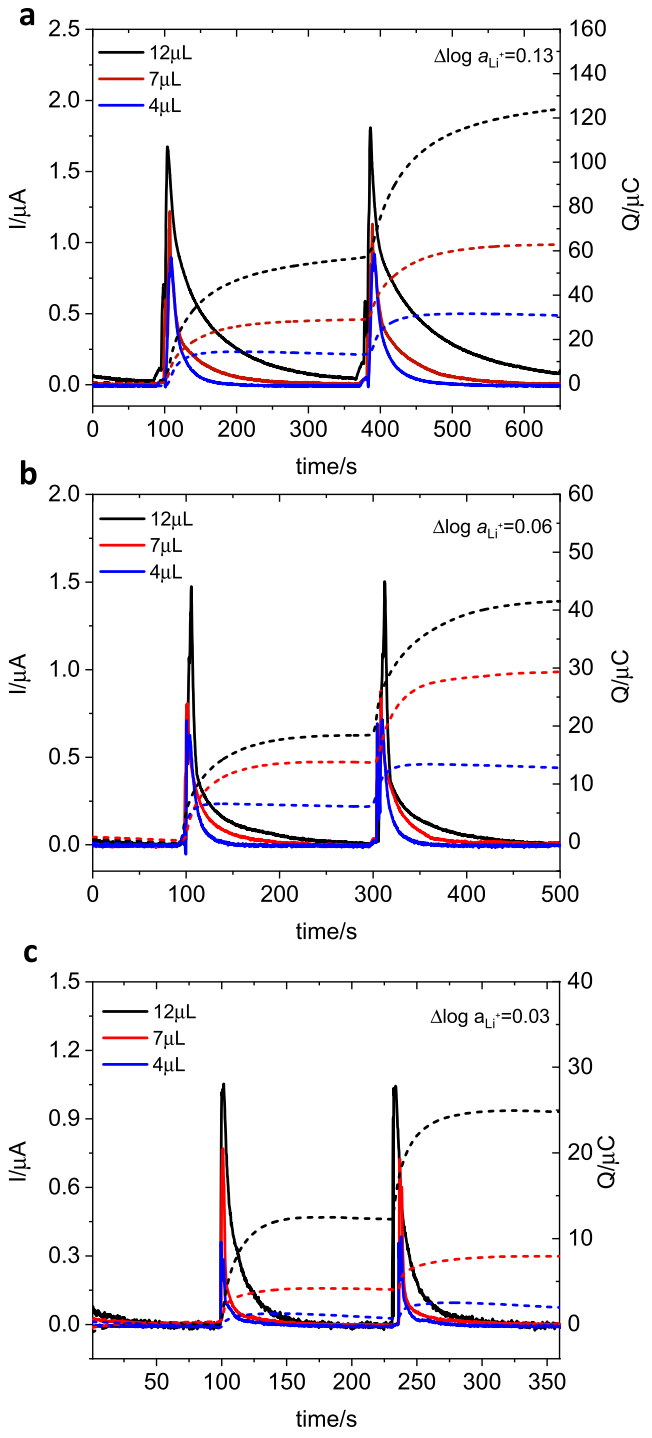

Fig. 3. Enlargement of chronoamperograms (solid lines) for GC/LMO electrodes and corresponding integrated charge Q (dashed lines) for different amounts of materials (12 μL, 7 μL, 4 μL) with (a) Δlog a_{Li+} = 0.13 dec/step, (b) Δlog a_{Li+} = 0.06 dec/step, (c) Δlog a_{Li+} = 0.03 dec/step. The starting concentration of the primary ion is 0.1 M LiCl.

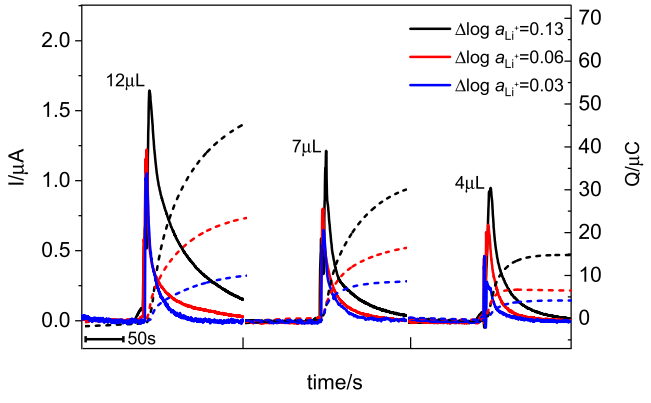

Fig. 4. Comparison of chronoamperograms (solid lines) and the corresponding integrated charge Q (dashed lines) for GC/LMO electrodes fabricated with different amounts of LMO (12 μL, 7 μL, 4 μL). The starting concentration of primary ion is 0.1 M LiCl.

Δlog a_{Li+}= 0.03 dec/step results in a relatively large current peak (0.7 μA) and Q (10 μC) within a response time of ca 1 min. This shows that the coulometric readout method is highly compatible with GC/LMO for detecting small concentration changes.

3.3. Reproducibility and reversibility of the coulometric response for GC/LMO

The reproducibility of the chronoamperometric and coulometric response for GC/LMO electrodes was evaluated by successive dilutions (Δlog a_{Li+} = 0.03 dec/step) of a starting solution of 0.1 M LiCl. The chronoamperometric (Fig. 5a) and coulometric (Fig. 5b) responses show good reproducibility, with only minor differences between individual GC/LMO electrodes. The relative standard deviation (%RSD) of the linearity for the integrated charge Q vs. ion activities between three individual electrodes was calculated to be 5.6%.

Fig. 5(c) and 5(d) show the reversibility of a GC/LMO electrode when switching between solutions of 0.1 M LiCl and 0.2 M LiCl. After conditioning in LiCl solutions, LMO equilibrates with the Li^+ concentration of the conditioning solution. Furthermore, the conditioning process in 0.1 M LiCl allows the LMO to be partially de-lithiated, so that the electrode can be used in both directions. The current peak recorded from 0.1 M to 0.2 M LiCl is −25 μA, while the reverse value is + 15 μA. These differences come from the different operating techniques used when changing the concentration of the solution to higher or lower values. The cumulative charge curve in Fig. 5(d) shows only a slight drift. Bearing in mind that the coulometric signal depends on the potential difference at the LMO/solution interface and the redox equilibrium of LMO, which involves intercalation/expulsion of Li^+ ions, the GC/LMO electrode can be considered to show good reversibility and reproducibility.

3.4. Selectivity of GC/LMO in the coulometric mode

Based on earlier potentiometric measurements [16], the GC/LMO electrode is expected to be highly selective to Li^+ vs. Na^+. Three fresh electrodes were fabricated to test the performance of GC/LMO in a mixed solution of 0.1 M LiCl and 0.1 M NaCl, where the latter was also used as a dilution electrolyte in the subsequent dilution steps (Fig. 6). Before the test, the GC/LMO electrodes were immersed in 0.1 M LiCl/NaCl mixed solution overnight. Reproducible peaks for three GC/LMO electrodes are shown in Fig. 6(a). After 9 dilutions with 0.1 M NaCl solution, the GC/LMO showed a linearity of −288.3 ± 30.6 μC/dec vs. Li^+ activities (Fig. 6b). Within the error bar, this value is the same as the linearity (-286.1 ± 15.6 μC/dec) tested in pure LiCl solution (Fig. 2b), which clarifies the selectivity of GC/LMO toward Li^+ in coulometric mode. We further conducted sensor selectivity measurements with respect to K^+, Ca^{2+}, and Mg^{2+} in their 0.1 M chloride solutions (Fig. 6c). The GC/LMO electrodes were conditioned in 0.1 M LiCl solution before the tests. The results show a much smaller transient current and integrated Q (<4 μC), compared with the curves in 0.1 M LiCl solution (Q = 59 μC), indicating that GC/LMO is significantly more selective to Li^+ than Na^+, K^+, Ca^{2+}, and Mg^{2+} ions, also in the coulometric mode.

The chronoamperometric response of GC/LMO without and with a plasticized PVC-based Li^+-selective membrane (GC/LMO/ISM) (Fig. S6) was compared in 0.1 M LiCl at Δlog a_{Li+} = 0.13 dec/step. As can be seen in Fig. S7, the GC/LMO produces an amperometric response (current peak of ca 1.5 μA) ca 65 times larger than the GC/LMO/ISM (current peak of ca 0.023 μA). The smaller response for GC/LMO/ISM can be

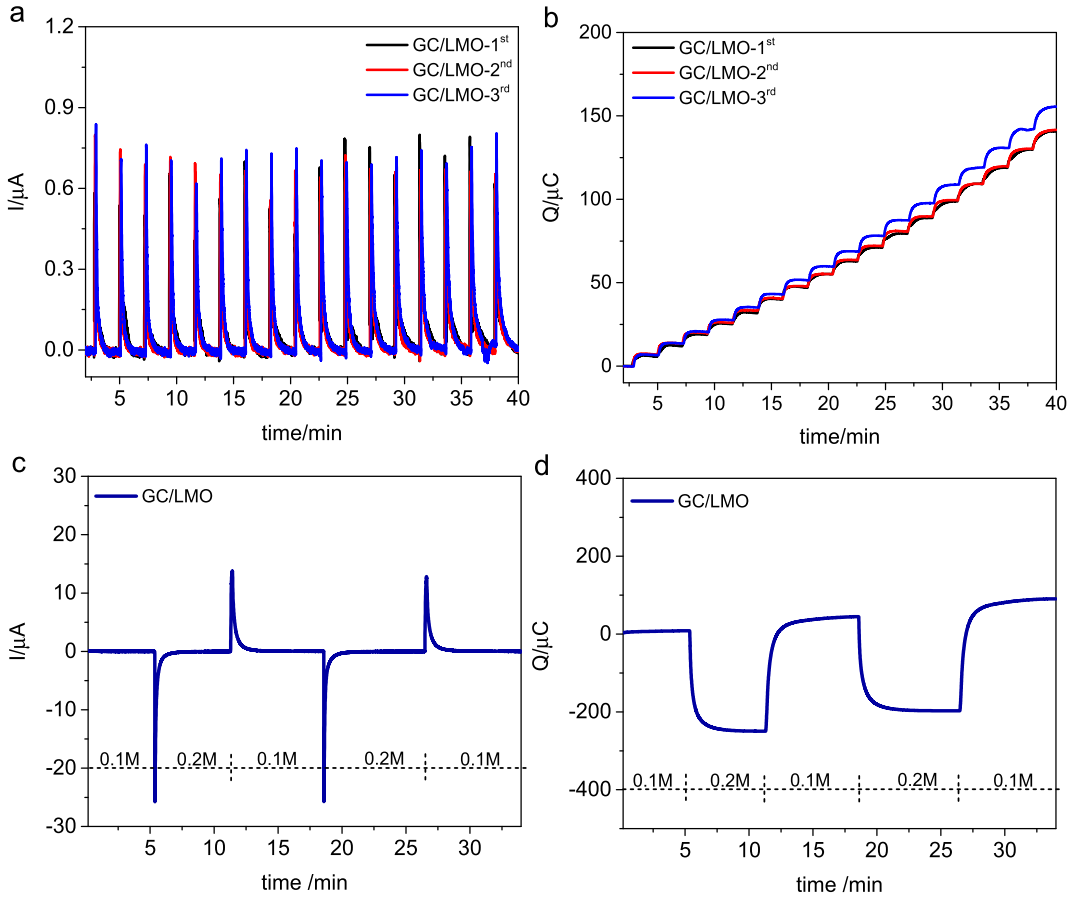

Fig. 5. Reproducibility and reversibility of the GC/LMO electrodes. (a) Chronoamperograms and (b) cumulative Q vs. time for three different GC/LMO electrodes with a mass loading of 12 μL. The starting solution was 0.1 M LiCl diluted with deionized water with Δlog a_{Li}^{+} = 0.03 dec/step. (c) Experimental current–time curve and (d) corresponding integrated charge curve recorded for the GC/LMO electrode in solutions of 0.1 M LiCl and 0.2 M LiCl, repeatedly.

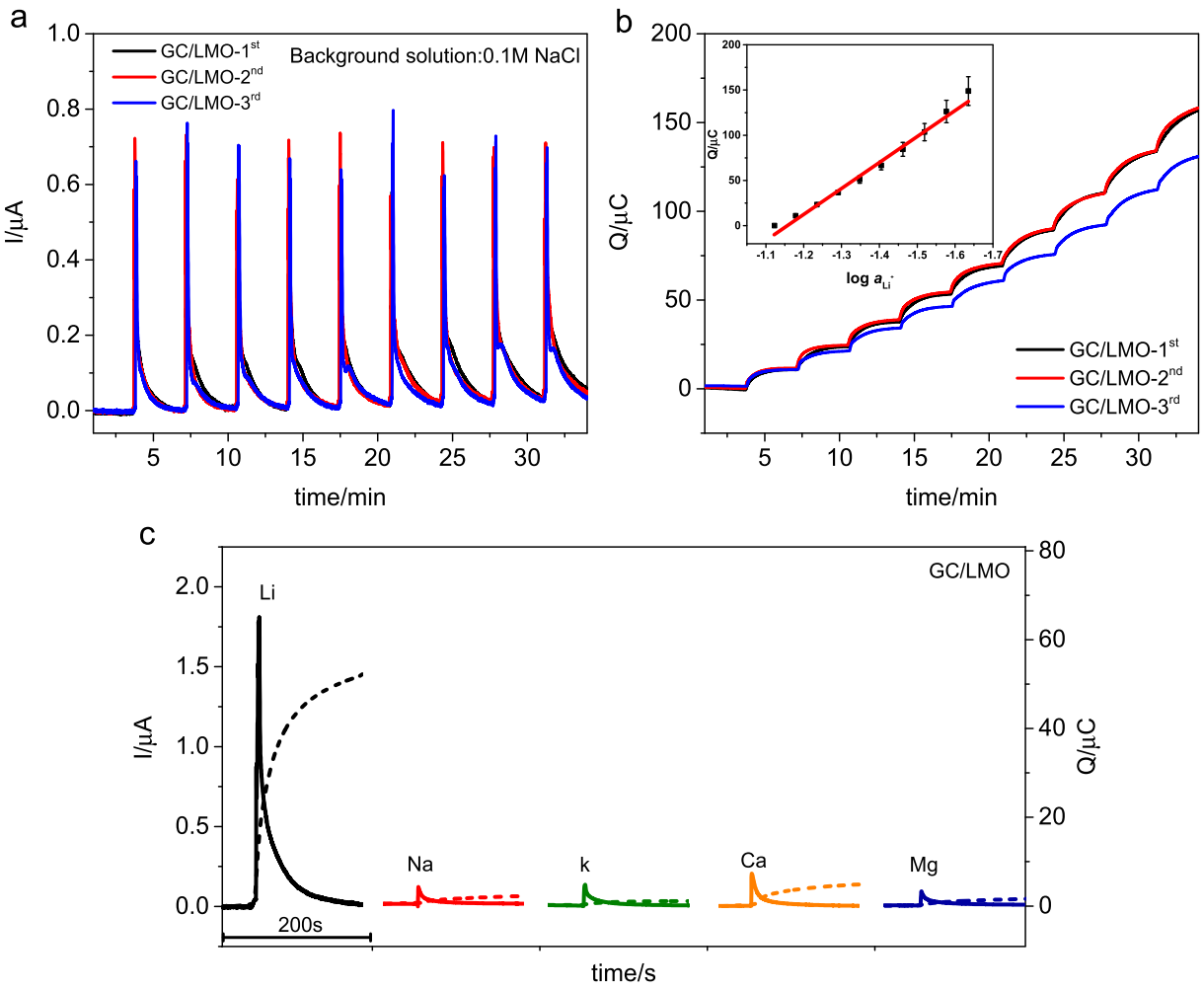

Fig. 6. Chronoamperograms (a) and the corresponding integrated charge Q (b) for GC/LMO-Li^+-ISEs, $\Delta\log a_{Li+} = 0.06$ dec/step, in which the inset image is the fitting line of Q vs. ion activities (n = 3). The starting solution was 0.1 M LiCl containing 0.1 M NaCl as constant background electrolyte. (c) Interference test for GC/LMO in the chloride solutions of 0.1 M Na^+, K^+, Ca^{2+}, Mg^{2+}, $\Delta\log a_{Li+} = 0.13$ dec/step, black line represents coulometric response of GC/LMO in 0.1 M LiCl solution.

related to the ion transport resistance of the plasticized PVC membrane of the GC/LMO/ISM. This demonstrates that the use of a membrane-free electrode, such as GC/LMO, significantly amplifies the current signal compared to a SC-ISE with a plasticized PVC membrane, and a decrease in chemical stability. Eliminating the PVC membrane reduces the overall resistance of the ISE, which brings great advantages when employing non-zero current electrochemical techniques, such as coulometry.

4. Conclusions

We have reported the coulometric signal readout method for a membrane-free ISE for the first time, using $LiMn_2O_4$ as the ion-recognition and transduction material. The mechanism of the coulometric response is analogous to that explored earlier for SC-ISEs, but the membrane-free ISE based on $LiMn_2O_4$ allows a higher amplification of the analytical signal. The coulometric response of $LiMn_2O_4$ to Li^+ ions displays excellent signal amplification and commendable reproducibility. Increasing the active area of $LiMn_2O_4$ gives a larger transient current signal and charge, but a longer response time. This is a characteristic feature of the coulometric transduction method. This work highlights the advantages of coulometric transduction for ion-selective electrodes based on electrode materials showing both ion-selectivity and ion-to-electron transduction properties.

CRediT authorship contribution statement

Yan Lyu: Methodology, Investigation, Formal analysis, Writing – original draft. **Tingting Han:** Formal analysis, Validation. **Lijie Zhong:** Formal analysis. **Yitian Tang:** Formal analysis. **Longbin Xu:** Formal analysis. **Yingming Ma:** Software, Resources. **Yu Bao:** Software, Resources. **Shiyu Gan:** Supervision, Conceptualization, Writing – review & editing. **Johan Bobacka:** Supervision, Conceptualization, Writing – review & editing. **Li Niu:** Project administration.

Declaration of Competing Interest

The authors declare that they have no known competing financial interests or personal relationships that could have appeared to influence the work reported in this paper.

Acknowledgments

This work was supported by the National Natural Science Foundation of China (21974032, U2006208 and 21974031), the Department of Science and Technology of Guangdong Province (2019B010933001) and the Science and Technology Research Project of Guangzhou (202102020622). Financial support by the Academy of Finland (project no. 317829) is gratefully acknowledged.

Appendix A. Supplementary data

Supplementary data to this article can be found online at https://doi.org/10.1016/j.elecom.2022.107302.

References

[1] H.Y.Y. Nyein, W. Gao, Z. Shahpar, S. Emaminejad, S. Challa, K. Chen, H.M. Fahad, L.-C. Tai, H. Ota, R.W. Davis, A. Javey, A wearable electrochemical platform for noninvasive simultaneous monitoring of Ca^{2+} and pH, ACS Nano 10 (7) (2016) 7216–7224.

[2] W. Gao, S. Emaminejad, H.Y.Y. Nyein, S. Challa, K. Chen, A. Peck, H.M. Fahad, H. Ota, H. Shiraki, D. Kiriya, D.-H. Lien, G.A. Brooks, R.W. Davis, A. Javey, Fully integrated wearable sensor arrays for multiplexed in situ perspiration analysis, Nature 529 (7587) (2016) 509–514.

[3] A. Alizadeh, A. Burns, R. Lenigk, R. Gettings, J. Ashe, A. Porter, M. McCaul, R. Barrett, D. Diamond, P. White, P. Skeath, M. Tomczak, A wearable patch for continuous monitoring of sweat electrolytes during exertion, Lab Chip 18 (17) (2018) 2632–2641.

[4] L. Mayerhuber, S. Trattner, S. Luger, G. Weigelhofer, C. Hametner, P. Fruhmann, Development of ion-selective electrodes for antipyrine and its derivatives as potential tool for environmental water monitoring, J. Electroanal. Chem. 886 (2021), 115110.

[5] A. Ceresa, E. Backer, B. Hattendorf, D. Günther, E. Pretsch, Potentiometric polymeric membrane electrodes for measurement of environmental samples at trace levels new requirements for selectivities and measuring protocols, and comparison with ICPMS, Anal. Chem. 73 (2001) 343–351.

[6] E.P. Bühlmann, E. Bakker, Carrier-based ion-selective electrodes and bulk optodes. 2. Ionophores for potentiometric and optical sensors, Chem. Rev. 98 (1998) 1593–1687.

[7] E. Bakker, P. Bühlmann, E. Pretsch, Carrier-based ion-selective electrodes and bulk optodes. 1. General characteristics, Chem. Rev. 97 (8) (1997) 3083–3132.

[8] E. Hupa, U. Vanamo, J. Bobacka, Novel ion-to-electron transduction principle for solid-contact ISEs, Electroanalysis 27 (3) (2015) 591–594.

[9] T. Han, U. Vanamo, J. Bobacka, Influence of electrode geometry on the response of solid-contact ion-selective electrodes when utilizing a new coulometric signal readout method, ChemElectroChem 3 (12) (2016) 2071–2077.

[10] P. Kraikaew, S.K. Sailapu, E. Bakker, Rapid constant potential capacitive measurements with solid-contact ion-selective electrodes coupled to electronic capacitor, Anal. Chem. 92 (20) (2020) 14174–14180.

[11] J. Bobacka, T. Lindfors, M. McCarrick, A. Ivaska, A. Lewenstam, Single-piece all-solid-state ion-selective electrode, Anal. Chem. 67 (20) (1995) 3819–3823.

[12] J. Bobacka, A. Ivaska, A. Lewenstam, Potentiometric ion sensors, Chem. Rev. 108 (2) (2008) 329–351.

[13] U. Vanamo, E. Hupa, V. Yrjänä, J. Bobacka, New signal readout principle for solid-contact ion-selective electrodes, Anal. Chem. 88 (8) (2016) 4369–4374.

[14] Y.O. Kondratyeva, E.G. Tolstopjatova, D.O. Kirsanov, K.N. Mikhelson, Chronoamperometric and coulometric analysis with ionophore-based ion-selective electrodes: A modified theory and the potassium ion assay in serum samples, Sens. Actuators B Chem. 310 (2020), 127894.

[15] Z. Jarolímová, T. Han, U. Mattinen, J. Bobacka, E. Bakker, Capacitive model for coulometric readout of ion-selective electrodes, Anal. Chem. 90 (14) (2018) 8700–8707.

[16] Y. Lyu, Y. Zhang, L. Xu, L. Zhong, Z. Sun, Y. Ma, Y.u. Bao, S. Gan, L.i. Niu, Solid-contact ion sensing without using an ion-selective membrane through classic Li-ion battery materials, Anal. Chem. 93 (21) (2021) 7588–7595.

[17] L. Xu, S. Gan, L. Zhong, Z. Sun, Y. Tang, T. Han, K. Lin, C. Liao, D. He, Y. Ma, W. Wang, L. Niu, Conductive metal organic framework for ion-selective membrane-free solid-contact potentiometric Cu^{2+} sensing, J. Electroanal. Chem. 904 (2022), 115923.

[18] C. Liao, L. Zhong, Y. Tang, Z. Sun, K. Lin, L. Xu, Y. Lyu, D. He, Y. He, Y. Ma, Y. Bao, S. Gan, L. Niu, Solid-contact potentiometric anion sensing based on classic silver/silver insoluble salts electrodes without ion-selective membrane, Membranes 11 (2021) 1–12.

[19] Y. Tang, S. Gan, L. Zhong, Z. Sun, L. Xu, C. Liao, K. Lin, X. Cui, D. He, Y. Ma, W. Wang, L. Niu, Lattice proton intercalation to regulate WO_3-based solid-contact wearable pH sensor for sweat analysis, Adv. Funct. Mater. 32 (2021) 2107653.

[20] Y. Lyu, S. Gan, Y. Bao, L. Zhong, J. Xu, W. Wang, Z. Liu, Y. Ma, G. Yang, L. Niu, Solid-contact ion-selective electrodes: response mechanisms, transducer materials and wearable sensors, Membranes 10 (2020) 1–24.

[21] M.M. Thackeray, K. Amine, $LiMn_2O_4$ spinel and substituted cathodes, Nat. Energy 6 (5) (2021), 566-566.

[22] Z. Li, X. Feng, L. Mi, J. Zheng, X. Chen, W. Chen, Hierarchical porous onion-shaped $LiMn_2O_4$ as ultrahigh-rate cathode material for lithium ion batteries, Nano Res. 11 (8) (2018) 4038–4048.

[23] T. Liu, A. Dai, J. Lu, Y. Yuan, Y. Xiao, L. Yu, M. Li, J. Gim, L. Ma, J. Liu, C. Zhan, L. Li, J. Zheng, Y. Ren, T. Wu, R. Shahbazian-Yassar, J. Wen, F. Pan, K. Amine, Correlation between manganese dissolution and dynamic phase stability in spinel-based lithium-ion battery, Nat. Commun. 10 (2019) 4721.

[24] A.L. Suherman, B. Rasche, B. Godlewska, P. Nicholas, S. Herlihy, N. Caiger, P. J. Cowen, R.G. Compton, Electrochemical detection and quantification of lithium ions in authentic human saliva using $LiMn_2O_4$-modified electrodes, ACS Sens. 4 (9) (2019) 2497–2506.

[25] M.-Y. Zhao, Z.-Y. Ji, Y.-G. Zhang, Z.-Y. Guo, Y.-Y. Zhao, J. Liu, J.-S. Yuan, Study on lithium extraction from brines based on $LiMn_2O_4/Li_{1-x}Mn_2O_4$ by electrochemical method, Electrochim. Acta 252 (2017) 350–361.

[26] Y. Wen, C. Ma, H. Chen, H. Zhang, M. Li, P. Zhao, J. Qiu, H. Ming, G. Cao, G. Tang, Stabilizing $LiMn_2O_4$ cathode in aqueous electrolyte with optimal concentration and components, Electrochim. Acta 362 (2020), 137079.

[27] J. Hedman, F. Björefors, Fiber optic monitoring of composite lithium iron phosphate cathodes in pouch cell batteries, ACS Appl. Mater. 5 (2021) 870–881.

[28] H. Wang, B. Yuan, T. Yin, W. Qin, Alternative coulometric signal readout based on a solid-contact ion-selective electrode for detection of nitrate, Anal. Chim. Acta 1129 (2020) 136–142.

[29] H. Kanoh, K. Ooi, Y. Miyai, S. Katoh, Electrochemical recovery of lithium ions in the aqueous phase, Sep. Sci. Technol. 28 (1-3) (1993) 643–651.

[30] M. Pasta, A. Battistel, F. La Mantia, Batteries for lithium recovery from brines, Energy Environ. Sci. 5 (2012) 9487–9491.

[31] G. Zhou, L. Chen, X. Li, G. Luo, Z. Yu, J. Yin, L. Fan, Y. Chao, L. Jiang, W. Zhu, Construction of truncated-octahedral $LiMn_2O_4$ for battery-like electrochemical lithium recovery from brine, Green Energy Environ. (2022), https://doi.org/10.1016/j.gee.2021.12.002.

[32] Y.-P. Lin, N.-L. Wu, Characterization of $MnFe_2O_4/LiMn_2O_4$ aqueous asymmetric supercapacitor, J. Power Sources 196 (2) (2011) 851–854.

[33] H. Manjunatha, K.C. Mahesh, G.S. Suresh, T.V. Venkatesha, The study of lithium ion de-insertion/insertion in $LiMn_2O_4$ and determination of kinetic parameters in aqueous Li_2SO_4 solution using electrochemical impedance spectroscopy, Electrochim. Acta 56 (3) (2011) 1439–1446.